University of Bath

Alternative formats
If you require this document in an alternative format, please contact:
openaccess@bath.ac.uk

Noninvasive, transdermal, path-selective and specific glucose monitoring *via* a graphene-based platform

Luca Lipani[1,2,4,5], Bertrand G.R. Dupont[1,2,4], Floriant Doungmene[1,4], Frank Marken[3,5], Rex M. Tyrrell[2], Richard H. Guy[2,4,5] & Adelina Ilie[1,4,5*]

Departments of Physics[1], Pharmacy & Pharmacology[2] and Chemistry[3], University of Bath, Claverton Down, Bath, BA2 7AY, U.K.
[4]Centre for Graphene Science, University of Bath, Bath, BA2 7AY, U.K.
[5]Centre for Nanoscience & Nanotechnology, University of Bath, Bath, BA2 7AY, U.K.

[*]Corresponding author: a.ilie@bath.ac.uk

Currently, a needle-free approach for diabetics to monitor glucose levels in the interstitial fluid (ISF) is not available. Here we report a path-selective, non-invasive, transdermal glucose monitoring system based on a miniaturised pixel array platform (realized either by graphene-based thin film technology, or screen-printing). The system samples glucose from the interstitial fluid via electro-osmotic extraction through individual, privileged, follicular pathways in the skin, accessible via the pixels of the array. Proof-of-principle using mammalian skin *ex-vivo* is demonstrated of specific and "quantized" glucose extraction/detection via follicular pathways, and across the hypo- to hyper-glycaemic range in humans. Furthermore, the quantification of follicular vs non-follicular glucose extraction fluxes is clearly shown. *In vivo* continuous monitoring of ISF-borne glucose with the pixel array was able to track blood sugar in healthy human subjects. This novel approach paves the way to clinically relevant glucose detection in diabetics without the need for invasive, "finger-stick" blood sampling.

The World Health Organization predicts the world-wide incidence of diabetes to increase from 171M in 2000 to 366M in 2030[1]. An essential feature of diabetic care is the frequent monitoring of blood glucose, conventionally via an invasive "finger-stick" procedure. This approach, however, suffers from significant user resistance, primarily due to pain and discomfort. The relatively recent development of implantable and microneedle-based temporary sensors[2-4] which are particularly important for very brittle Type 1 diabetics, is not a suitable or economically viable solution for the much larger (and rapidly growing) number of Type 2 sufferers of the disease[5]. Non-invasive methods have been proposed involving, for example, detection of glucose in sweat[6-8] or tears[9,10] or saliva[11] but these strategies have two limitations: (a) significant variability in the level of glucose detected, and (b) the unknown proportionality between the measured glucose concentration in these fluids to that in the blood. Inevitably, therefore, calibration via a "finger-stick" is required. Impedance and spectroscopic (e.g., infrared) techniques have also been examined[12-14] but, in addition to the calibration challenge, these methods suffer from interference and a consequent lack of specificity.

The only technology to offer non-invasive, continuous glucose monitoring used reverse iontophoresis (RI) to extract interstitial fluid (ISF) though the skin via electro-osmosis[15]. This approach was embodied in the GlucoWatch Biographer®[16,17], which received U.S. Food & Drug Administration approval in 2001. In this method, a small electric field is applied across the skin causing ion flow to occur. Because, under normal physiological conditions, the skin is net negatively charged, there is an electroosmotic flow of ISF from within the skin towards the cathode on the skin surface[18], where glucose is detected and quantified. The GlucoWatch® exploited the known correlation between ISF and blood glucose concentrations[19,20] (and the inter-individual consistency of the overlap between glucose levels in the ISF and capillary and venous blood levels during rapid changes in glycaemia[21-23]) to provide essentially

continuous monitoring of blood sugar for up to 12 hours. However, a "finger-stick" calibration remained a requirement primarily because glucose was extracted indiscriminately and variably across a relatively large area of skin (>3 cm^2) and underwent substantial dilution before quantification. Therefore, the device did not exploit the fact that most of the electroosmotic flow during iontophoresis follows low resistance, preferential pathways associated primarily with hair follicles[24-26]. This is the basis for the concept proposed and tested here (Figure 1(a)): to create a device with an array of miniature 'pixels', into some of which the ISF drawn through the skin electro-osmotically is captured into a known, small volume permitting the *calibration-free* detection of systemic glucose concentration. This is achieved by fixing the pixel's area and volume so that the dilution factor of the extracted glucose is constant and *independent of follicular density* (Supplementary, Figure S1). Given the range of hair densities in humans on conveniently accessible sites on the body (e.g., 18 to 36 hairs/cm^2 on the arms, thorax, thighs[27]), a correctly chosen array ensures that the majority of individual pixels interrogate a single preferred pathway, that a redundancy of these pathways can be interrogated (Figure 1(b), and Supplementary, Figure S2), and that the variability in detection seen with the GlucoWatch® (and a more recent "tattoo"-type version thereof[28]) can be avoided and the "finger-stick" calibration requirement relaxed.

Path-selective glucose monitoring platform: concept

A miniature, individual pixel of such an array, embodying/achieving this principle comprises (Figure 2 (a)): (i) a glucose oxidase-bearing hydrogel reservoir, into which glucose is extracted transdermally, (ii) an electrochemical glucose sensor, specifically a graphene-based film decorated with platinum nanoparticles for enhanced sensitivity, and (iii) miniaturized electrodes suitable for sensor electrochemistry and reverse iontophoresis, all supported by a flexible substrate. The first-generation prototype we produced relied on thin film technology, including chemical vapour deposition (CVD) graphene incorporated in a Pt nanoparticle-graphene hybrid material. Graphene is the preferred material because of its mechanical resilience, high conductivity and low capacitive background[29], large surface area, suitability for patterning and device integration via standard microfabrication techniques[30], environmental sustainability, and anticipated low cost[30,31] (relative to the use of noble metals) in a commercial product. A second-generation prototype used commercially-available screen printing and ink-based (including a graphene ink) electrodes. Glucose extracted by reverse iontophoresis reacts with glucose oxidase producing hydrogen peroxide, which is detected by the electrochemical sensor. Crucially, the active area of the pixel device (into which glucose is extracted) enables access to a single follicular pathway. Assuming an average follicular density of 27 follicles per cm^2 (at the sites mentioned above[27]), an active area of 2-6 mm^2 maximises the probability of hitting a single follicle in a randomly-positioned, untargeted measurement (Figure 1(b), panel 1). A 4 x 4 array of pixels guarantees at least one follicular "hit", while larger arrays ensure useful redundancy (Figure 1(b), panels 1 and 2, and Supplementary, Figures S2 and S3). Further, restricting the pixel active area to 2-5 mm^2 ensures the dominance of single follicular hits per pixel across the follicular density range of 18 to 36 hairs/cm^2 (Figure 1(b), panel 2, and Supplementary, Figures S2 and S3). The gel volume in a pixel additionally determines the extent of dilution of the extracted glucose, and hence the concentration range over which the sensor operates.

To provide proof-of-principle, we first tested a deconstructed individual pixel device (Figure 2(b)), where a detachable gel reservoir was placed on top of excised porcine skin (an excellent model for the human skin barrier[32,33]) and into which glucose was extracted. Subsequently, the reservoir was transferred onto a Pt nanoparticle-decorated graphene electrode for glucose detection. Both extraction and detection circuits were completed by miniaturized wire electrodes to provide a more customary, three-dimensional geometry for benchmarking measurements. In this way, dual glucose extraction-detection through single follicular pathways using miniature pixel geometries was demonstrated, and both follicular and non-follicular glucose extraction fluxes were quantified. Second, a 2 x 2 pixel

array was created with all elements integrated on a flexible substrate (Figure 2(c)) following the concept design and geometric requirements outlined above, and the pixels' performance was compared with that obtained with the three-dimensional geometry. A first-generation prototype, based on thin film technology and CVD graphene, demonstrated all functional aspects of the array. In particular, *ex-vivo,* porcine skin-based experiments enabled direct visualisation of the follicular pathways probed and, using specific subdermal glucose concentrations, showed that the glucose detection current (the output of an extraction-detection cycle) is "quantized", with a "quantum" corresponding to the read-out from a single follicular pathway. Finally, a second-generation prototype 2 x 2 pixel array of similar architecture, but based entirely on screen printing (including a graphene ink), was then used to demonstrate the concept *in-vivo* in healthy human subjects.

Operational characteristics of an individual pixel

Response to glucose: deconstructed sensor

Figure 3(a) displays the electrochemical current *vs* glucose concentration calibration curve of a 3 x 3 mm^2 Pt nanoparticle-decorated CVD graphene sensor measured with the three-dimensional set-up in Figure 2(b), panel 2. In this experiment, glucose was presented to the sensor in a 24 μL enzyme-encasing gel reservoir. Data were obtained from the sensor's chronoamperometric response, at an operational potential of 0.4 V, to a wide range of concentrations, from sub-micromolar to more than millimolar (Supplementary, Figure S6). A sensitivity of ~2.2 μA mM^{-1} cm^{-2} was determined, with a limit of detection (LoD) of 2.8 μM (Methods).

For specific RI extraction conditions (i.e., extraction current, current density and time of 0.2 mA, ~ 2.2 mA/cm^2 and 1 hour, respectively), the hypo- to hyper-glycaemic range in diabetics (3.5-12 mM in the blood[34]), after dilution within the reservoir gel volume, maps completely onto the sensor calibration curve (Figure 3(a)). The corresponding glucose concentration range in the gel was 8-25 μM (Methods), well above the sensor's LoD. Clearly, a significant decrease in reservoir volume (e.g., to the μL range), while maintaining the same operational concentration range, proportionally decreases the glucose extraction current and time. This informed the further design and operational parameters of the individual pixel devices within the planar array.

Follicular vs non-follicular glucose extraction fluxes

The *preferential* RI extraction of glucose through hair follicles was first established in two experiments using the deconstructed configuration (Figure 2(b)): first, via hair "targeting", where the miniature gel "pixel" was positioned directly on a single hair follicle and, second, by comparing extraction across skin samples with varying amounts of hair. In both experiments, RI was conducted under the same conditions on two skin samples with different follicular densities; identical gel reservoir volumes (24 μL) were used and the electrochemical detection of glucose therein was performed with the *same* graphene sensor. This approach employed the experimental configuration in Figure 2(b), with the gel "pixel" not yet permanently integrated with the graphene sensor. Single-follicle, "hair-targeted", preferential extraction on a skin sample with 34 hairs/cm^2 was compared with that from another that was relatively devoid of follicles (6 hairs/cm^2), and the relative RI extraction fluxes via follicular and non-follicular pathways were estimated. For this, the chronoamperometric curves obtained after glucose extraction are used to determine an average detection current (Figure 3(b), panel 1) which, when interpolated on the current-concentration calibration curve of the sensor, provides the extracted glucose concentration within the pixel gel (Figure 3(b), panel 2) and hence the glucose extraction flux (Methods).

At a subdermal concentration of 10 mM, glucose flux via the preferential pathways was 3.5 nmol mA^{-1} hr^{-1}, compared to that across non-follicular skin of 0.4 nmol mA^{-1} hr^{-1}. These values are consistent with the glucose extraction flux (4.5 nmol mA^{-1} hr^{-1}) across porcine skin *ex vivo* calculated from large area extraction experiments reported earlier[24].

More importantly, they agree with data from the planar pixel arrays developed next (Figures 4 and 5). The preferential pathway result also concurs with direct observations of enhanced follicular electro-transport of hydroquinone and the independent quantification of electro-osmosis using scanning electrochemical microscopy[26]. The research described here, however, represents the first direct demonstration of extraction and quantitative detection at a single follicle level using a technology platform compatible with the construction of a fully integrated glucose monitor.

The electrochemical detection of glucose described above was independently validated by quantitative [1]H-nuclear magnetic resonance (^{1}H-qNMR)[35] (Supplementary, Figure S8 and Tables S1-S2).

A 2 x 2 pixel array on a flexible substrate

Figure 4 compiles representative *ex-vivo* extraction-detection experiments with three different 2 x 2 thin film/ CVD graphene-based arrays as described above, and compatible with a final implementation (Figures 4(a) and 1(b)). The volume of the pixel gel reservoirs was significantly reduced to 1- 2 μL enabling the array's operational parameters to be appropriate for realistic usage: e.g., 5-minute periods of extraction, at a current density of ~ 0.5 mA/cm^2. The outcome is an operational range (Methods) for the glucose concentration in the pixel gel indicated by the purple area in Figure 4(c), panel 1. With an increased density of graphene-decorating Pt nanoparticles, the detection current normalised to the macroscopic area of the sensing electrode is more than an order of magnitude greater than that for the deconstructed, three-dimensional pixel device (Supplementary, Figure S14): that is, the sensitivity increases to 37 μA mM^{-1} cm^{-2}, while the LoD is improved to about 0.76 μM (Figure 4(b), panel 1). Viability of the array design was also demonstrated using gold (a more conventional sensing material) and resulted in very similar calibration curves to CVD graphene when integrated in an identical array design (compare Figure 4(c), panel 1 with Figure S15, Supplementary).

As detailed below, the Pt nanoparticle - CVD graphene array demonstrated all the required functional aspects: (i) lack of response to interfering species in real-life conditions (Figure 4(b), panel 2, and Supplementary, Figure S12), (ii) targeted extraction (Figures 4 (c-d)), (iii) correlation and proportionality with the number of hair follicles probed by the respective pixels (Figures 4 (c-d)), (iv) capability to detect glucose extracted through a single hair follicle (Figure 4(d)), (v) proportionality with the concentration of subdermal glucose (Figure 4(c), panel 3; see also Figure 5(a)), and (vi) close operational characteristics of pixels both within an array and between different arrays (Figures 4(c), panel 1 and Supplementary, Figure S10).

A number of potential interfering species can be found in the ISF, such as acetaminophen and ascorbic acid (up to 0.1 mM[36,37]) and uric acid (up to 0.25 mM[38]). Uric and ascorbic acids are negatively charged and are therefore extracted to the anode, i.e., the opposite electrode to that where glucose is found (electro-osmotic flow across the net negatively-charged skin carrying neutral compounds to the cathode, of course - Figure 2(b), panel 1). Only acetaminophen (also uncharged), therefore, is a potential interfering species for glucose. Supplementary, Figures S12, and S13 demonstrate the lack of response of the array sensor to all of these species.

For glucose extraction, the reverse iontophoresis extraction circuit employs the largest of the Ag/AgCl electrodes (labelled 1 on Figure 4(a)), located on two adjacent pixel devices, as the anode and cathode. In this configuration, during half of the operation cycle, glucose is extracted into one of the pixels while, in the second half, the direction of the extraction current is reversed, and glucose is extracted in the other pixel. In this way, the AgCl content of the extraction electrodes remains essentially constant (Methods).

Figure 4(c), panel 2 shows the set of chronoamperometric detection curves obtained after extraction via each of the pixels of an array (for which sensitivity calibration curves are in Figure 4(c), panel 1); each pixel probed a certain number of follicular pathways, determined by visual inspection. Each of these chronoamperometric curves was

analysed in a manner similar to that utilized in Figure 3(b): the time-averaged read-out current between 50 and 600 seconds was used with the current-concentration calibration curve of the respective pixel (from Figure 4(c), panel 1) to obtain, by interpolation, the concentration of glucose extracted within the pixel. The glucose concentration thus determined is "quantized", i.e., proportional to the number of follicles probed by each pixel. To simply convey this result, the inset of Figure 4(c), panel 2, relates the four read-out average currents of the array to these quantized concentration values *via* the average of the four calibration curves from panel 2 (instead of showing, for each pixel, its individual calibration curve, as used in the actual analysis). Figure 4(d) shows chronoamperometric detection curves, correlated with images of the hair follicles targeted by the pixels of an array, to show how the extraction-detection is practically performed. In this case, detection after extraction through a single follicle could also be probed, corresponding to the "quantum" of extracted glucose concentration. Measuring all pixel devices across all three arrays in Figure 4 yielded "quanta" of 18.9 ± 2.1 μM glucose in the pixel gel and 8.97 ± 1.01 nA read-out current per follicle, for a 5-minute period of extraction into a 1 μL gel, at 0.5 mA/cm^2 RI current density, and with 10 mM glucose subdermally. This is consistent with a glucose follicular extraction flux of 4.6 ± 0.5 nmol mA^{-1} hr^{-1}, a value slightly higher than that determined with the deconstructed pixel and possibly attributable to the different two- and three-dimensional geometries used. Furthermore, extraction via non-follicular skin in similar conditions results in a detected current that decays much faster than that observed after follicular extraction (Figure 4(c), panel 2), due to the very low glucose content within the pixel gel. Taken together, these experiments unequivocally demonstrate that the array operates as designed, by exploiting the hair follicles as the preferential transdermal extraction paths for glucose. In addition, Figure 4(c), panel 3 shows that, after extraction to the same pixel device under identical conditions, the detected current is proportional to the subdermal glucose concentration (10 and 100 mM were used here; see also Figure 5(a)).

In-vivo monitoring with a 2x2 screen printed array

In preparation for *in-vivo* experiments, similar *ex-vivo* measurements were extended to a prototype, second-generation, screen-printed array, based on the same architecture as the thin-film/CVD graphene-based arrays above. The CVD graphene working electrodes of the first-generation arrays were replaced with graphene ink-based electrodes, decorated with Pt nanoparticles. The first and second generation prototypes have close operational characteristics as shown, for example, by their calibration (Supplementary, Figure S14) and chronoamperometric curves (Figures 4 and 5(a)). The screen-printed arrays are expected to sustain more extraction/detection cycles (suitable for continuous *in-vivo* use) than those based on thin films due to the 6-fold increase in Ag/AgCl electrode thickness (Methods).

The read-out current of screen-printed pixel devices in *ex-vivo* experiments (determined from the chronoamperometric curves by averaging, as above) was proportional to the subdermal glucose concentration across the entire hypo- to hyper-glycaemic range (Figure 5(a), panels 1 and 2); and a plot (Figure 5(a), panel 3) of read-out current as a function of expected values of in-gel extracted concentration (C_1^* to C_4^*, as calculated using the same extraction/detection conditions as for the CVD graphene-based arrays, the follicular flux determined from Figure 4, and the four subdermal concentrations used for extraction) maps very well onto the calibration curve of the device. A conversion factor F (characteristic of the current pixel device architecture and extraction conditions, see Methods) from the subdermal glucose concentration to that in 1 μL of pixel gel, and per follicular pathway, of the order of 2.4×10^{-3} was then determined.

Finally, *in-vivo* testing was performed on two healthy volunteers, and representative results are in Figure 5(b). Panel 1 shows the wired array strapped to the volunteer's forearm (see also Supplementary, Figure S17). Glucose was

monitored over 6 hours, during which "lunch" and a "snack" were ingested (Figure 5(b), panel 3). The blood glucose was tracked using a commercial glucose meter (Accu-Chek® Mobile). In parallel, RI-extracted ISF-borne glucose was monitored by two of the array's pixel devices working in tandem (see Methods and above), and produced well-matched read-out values that provided further confidence in the performance of the array. The ISF glucose profile closely follows that of blood glucose, with a lag of about 15 minutes, as expected[19,39]. Importantly, control experiments show that, without RI, no glucose was detected (Supplementary, Figure S16), confirming that, under normal transdermal monitoring conditions, i.e., when the user is not actively perspiring (e.g., due to strenuous exercise or high ambient temperatures), there is no contamination of the ISF-borne glucose by that in the sweat. Nonetheless, it is essential that future development of the approach described characterises, in comprehensive clinical experiments, the response of the device to the full range of hypo- to hyper-glycaemia in diabetics, as well as that, for example, in individuals undertaking physical activity or exposed to rapid changes in environmental conditions (such as leaving an air-conditioned office into a high humidity and temperature outside).

Conclusions

Proof-of-concept is demonstrated for non-invasive, transdermal, *path-selective* and specific glucose monitoring, based on an array of miniature pixel devices integrated on a flexible substrate. In this way, interstitial fluid-borne glucose *via* individual, privileged follicular pathways across the skin is extracted and detected, producing "quantized" read-outs of subdermal glucose. The concept is founded on the array architecture rather than the specific sensor implementation. Pixel arrays (2 x 2) on mammalian skin *ex-vivo* enabled the evaluation and demonstration of all critical parameters and functional aspects of the monitor, and future work focuses on extending the array size to at least 4 x 4 (to ensure random sampling of single follicles). *In-vivo* testing on healthy human subjects demonstrated the ability to continuously track blood sugar for 6 hours, and extending this operation time is an ongoing objective. Graphene-supported platforms (e.g., incorporating CVD graphene, or graphene inks via screen printing, as shown here) are preferred implementations for cheap, flexible, high-throughput and green arrays. Unlike other "wearable" approaches for glucose monitoring, the technology described here should ensure that the relationship between measurements made by the device and the actual blood glucose concentrations is not subject to inter- and intra-individual fluctuations in skin characteristics. This achievement should pave the way to *calibration-free* non-invasive glucose monitoring.

References

1. Wild, S., Roglic, G., Green, A., Sicree, R. & King, H. Global prevalence of diabetes. *Estimates for the Year 2000 and Projections for 2030* **27,** 1047-1053 (2004).

2. McGarraugh, G., Brazg, R. & Weinstein, R. Freestyle Navigator continuous glucose monitoring system with Trustart algorithm, a 1-hour warm-up time. *J. Diabetes Sci. Technol.* **5,** 99-106 (2011).

3. Mamkin, I., Ten, S., Bhandari, S. & Ramchandani, N. Real-time continuous glucose monitoring in the clinical setting: the good, the bad, and the practical. *J. Diabetes Sci. Technol.* **2,** 882-889 (2008).

4. Torjman, M. C., Dalal, N. & Goldberg, M. E. Glucose monitoring in acute care: technologies on the horizon. *J. Diabetes Sci. Technol.* **2,** 178-181 (2008).

5. Burge, M. R., Mitchell, S., Sawyer, A. & Schade, D. S. Continuous glucose monitoring: the future of diabetes management. *Diabetes Spectr.* **21,** 112-119 (2008).

6. Olarte, O., Chilo, J., Pelegri-Sebastia, J., Barbe, K. & Van Moer, W. Glucose detection in human sweat using an electronic nose. *Conf. Proc. IEEE Eng. Med. Biol. Soc.* **2013,** 1462-1465 (2013).

7. Lee, H. et al. A graphene-based electrochemical device with thermoresponsive microneedles for diabetes monitoring and therapy. *Nat. Nanotechnol.* **11,** 566-572 (2016).

8. Heikenfeld, J. Non-invasive analyte access and sensing through eccrine sweat: challenges and outlook circa 2016. *Electroanalysis* **28,** 1242-1249 (2016).

9. Yan, Q. et al. Measurement of tear glucose levels with amperometric glucose biosensor/capillary tube configuration. *Anal. Chem.* **83,** 8341-8346 (2011).

10. Yao, H., Shum, A. J., Cowan, M., Lähdesmäki, I. & Parviz, B. A. A contact lens with embedded sensor for monitoring tear glucose level. *Biosens. Bioelectron.* **26,** 3290-3296 (2011).

11. Zhang, W., Du, Y. & Wang, M. L. Noninvasive glucose monitoring using saliva nano-biosensor. *Sens. Biosensing Res.* **4,** 23-29 (2015).

12. Yeh, S.-J., Hanna, C. F. & Khalil, O. S. Monitoring blood glucose changes in cutaneous tissue by temperature-modulated localized reflectance measurements. *Clin. Chem.* **49,** 924 (2003).

13. Weinzimer, S. A. Analysis: Pendra: The once and future noninvasive continuous glucose monitoring device? *Diabetes. Technol. Ther.* **6,** 442-444 (2004).

14. Yu, S. et al. In vitro glucose measurement using tunable mid-infrared laser spectroscopy combined with fiber-optic sensor. *Biomed. Opt. Express* **5,** 275-286 (2014).

15.   Potts, R. O., A. Tamada, J. & J. Tierney, M. Glucose monitoring by reverse iontophoresis. *Diabetes Metab. Res. Rev.* **18,** S49-S53 (2002).

16.   Tierney, M. J., Electrochemical sensor with dual purpose electrode. Patent http://patft.uspto.gov/netacgi/nph-Parser?Sect1=PTO1&Sect2=HITOFF&d=PALL&p=1&u=%2Fnetahtml%2FPTO%2Fsrchnum.htm&r=1&f=G&l=50&s1=5954685.PN.&OS=PN/5954685&RS=PN/5954685 (1999).

17.   Sage, B. H., Jr. FDA panel approves Cygnus's noninvasive GlucoWatch. *Diabetes. Technol. Ther.* **2,** 115-116 (2000).

18.   Marro, D., Kalia, Y. N., Delgado-Charro, M. B. & Guy, R. H. Contributions of electromigration and electroosmosis to iontophoretic drug delivery. *Pharm. Res.* **18,** 1701-1708 (2001).

19.   Boyne, M. S., Silver, D. M., Kaplan, J. & Saudek, C. D. Timing of changes in interstitial and venous blood glucose measured with a continuous subcutaneous glucose sensor. *Diabetes* **52,** 2790 (2003).

20.   Garg, S. K. et al. Correlation of fingerstick blood glucose measurements with GlucoWatch Biographer glucose results in young subjects with type 1 diabetes. *Diabetes Care* **22,** 1708-1714 (1999).

21.   Basu, A. et al. Time lag of glucose from intravascular to interstitial compartment in humans. *Diabetes* **62,** (2013).

22.   Rebrin, K. & Steil, G. M. Can interstitial glucose assessment replace blood glucose measurements? *Diabetes. Technol. Ther.* **2,** 461-472 (2000).

23.   Wang, P. M., Cornwell, M. & Prausnitz, M. R. Minimally invasive extraction of dermal interstitial fluid for glucose monitoring using microneedles. *Diabetes. Technol. Ther.* **7,** 131-141 (2005).

24.   Sieg, A., Guy, R. H. & Delgado-Charro, M. B. Electroosmosis in transdermal iontophoresis: implications for noninvasive and calibration-free glucose monitoring. *Biophys. J.* **87,** 3344-3350 (2004).

25.   Turner, N. G. & Guy, R. H. Visualization and quantitation of iontophoretic pathways using confocal microscopy. *J. Invest. Dermatol. Symp. Proc.* **3,** 136-142

26.   Bath, B. D., White, H. S. & Scott, E. R. Visualization and analysis of electroosmotic flow in hairless mouse skin. *Pharm. Res.* **17,** 471-475 (2000).

27.   Otberg, N. et al. Variations of hair follicle size and distribution in different body sites. *J. Invest. Dermatol.* **122,** 14-19 (2004).

28. Bandodkar, A. J. et al. Tattoo-based noninvasive glucose monitoring: a proof-of-concept study. *Anal. Chem.* **87,** 394-398 (2015).

29. Alshammari, A. et al. A modular bioplatform based on a versatile supramolecular multienzyme complex directly attached to graphene. *ACS Appl. Mater. Interfaces* **8,** 21077-21088 (2016).

30. Bae, S. et al. Roll-to-roll production of 30-inch graphene films for transparent electrodes. *Nat. Nanotechnol.* **5,** 574-578 (2010).

31. Graphenea. The price of graphene. https://www.graphenea.com/pages/graphene-price (2013).

32. Schmook, F. P., Meingassner, J. G. & Billich, A. Comparison of human skin or epidermis models with human and animal skin in in-vitro percutaneous absorption. *Int. J. Pharm.* **215,** 51-56 (2001).

33. Sekkat, N. & Guy, R. H. Biological models to study skin permeation. *Pharmacokinetic Optimization in Drug Research*, 155-172 (Verlag Helvetica Chimica Acta, Zurich, 2007).

34. Diabetes UK. Blood sugar level ranges. http://www.diabetes.co.uk/diabetes_care/blood-sugar-level-ranges.html (2017).

35. Pauli, G. F., Gödecke, T., Jaki, B. U. & Lankin, D. C. Quantitative 1h NMR. Development and potential of an analytical method: an update. *J. Nat. Prod.* **75,** 834-851 (2012).

36. *Chemical and Biological Microsensors: Applications in Fluid Media* (Wiley-ISTE, London, 2009).

37. *ICH Harmonised Tripartite Guideline* (International Conference On Harmonisation Of Technical Requirements For Registration Of Pharmaceuticals For Human Use, Geneva, 2005).

38. *Electrochemical Sensor Analysis* (Elsevier Science, Amsterdam, 2007).

39. Tamada, J. A. et al. Noninvasive glucose monitoring: comprehensive clinical results. *JAMA* **282,** 1839-1844 (1999).

Author Contributions

AI, RHG, and RMT designed the overall work program. BGRD performed the work related to the deconstructed pixel device. LL and FD performed the work related to the planar thin film/CVD graphene pixel array integrated on a flexible substrate. LL performed the work related to the screen-printed arrays, with input from FD. FM provided advice on the implementation of the electrochemistry experiments. AI rationalized the array characteristics via simulations, while AI and FD proposed the detailed pixel array architecture (for both generations, thin film and screen printed, of prototypes). AI, RHG and RMT supervised the deconstructed pixel device research, while AI and RHG supervised the pixel array research. AI and RHG wrote the paper, while all authors provided comments and agreed with the final form of the manuscript.

Additional Information

Supplementary information is available in the online version of the paper. Reprints and permission information is available online at www.nature.com/reprints. Correspondence and request of materials should be addressed to A. Ilie.

Figure captions

Figure 1. **Principle of a pixel-based array targeting transdermal individual preferential glucose pathways.** (a) Preferential glucose pathways (i.e., hair follicles) are targeted by individual, miniature pixel extraction-detection devices. With a sufficiently dense pixel array and the correct pixel size, a number of such pathways are sampled randomly and *individually* by the pixel devices. In this way, the concentration of glucose extracted via the hair follicles is in a fixed relationship to that in the interstitial fluid (ISF). (b) Panel 1: Probability P that the array has at least one working pixel with just a single pathway per pixel (calculated at 27 follicles/cm^2; i.e. the median value across a typical follicular density range at easily accessible skin sites in humans), as a function of pixel *active area* and for various numbers of pixels in the array. Here, the *active area* is defined as the pixel device area through which glucose extraction takes place, coinciding with the footprint area of the gel reservoir (see Figures 2 (a), (c)). Panel 2: Probability P as a function of pixel active area for a 4×4 array for three selected follicle densities spanning the follicular density over a wide range of suitable sites, e.g. arm, back and thigh. A common range of pixel areas exists that guarantees interrogation of individual follicular pathways at these convenient body regions.

Figure 2. **Individual pixel and array concept; extraction-detection operation cycle.** (a) Generic individual miniature pixel: electrodes 1 (Ag/AgCl) and 4 (Ag) perform glucose extraction; electrodes 1 (Ag/AgCl, reference), 2 (Pt nanoparticle-decorated graphene, working electrode), and 3 (Pt, counter electrode) detect glucose electrochemically. Pt nanoparticles on graphene boost the detection signal. Electrodes 1, 2 and 3 contact a miniaturized enzyme-encasing gel reservoir, into which glucose is extracted, and the area of which defines the pixel *active area*. The gel reservoir is formed inside the holes of a supporting elastomer membrane. (b) Deconstructed,

three-dimensional pixel configuration. Panel 1: Glucose extraction by reverse iontophoresis (RI). Excised porcine skin separates the two halves of a Franz diffusion cell, with the epidermal side facing the upper compartment; the lower, sub-dermal compartment contains glucose in phosphate-buffered saline (PBS), and hosts a silver anode. The enzyme-containing gel reservoir is positioned on the skin surface, with the Ag/AgCl cathode contacting the gel. As mammalian skin carries a net negative charge at pH 7.4, iontophoresis (red arrow) induces electro-osmosis, and the transport of glucose (G) in the direction of cation migration. Panel 2: Glucose sensing. After extraction, the gel is placed on top of the pixel-sized graphene sensor, and a three-dimensional electrochemical cell is formed by contacting the gel with Ag/AgCl (reference) and Pt (counter) electrodes. (c) Planar 2×2 array, on a flexible substrate, performing non-invasive glucose extraction-detection *ex vivo* (on porcine skin). For simplicity, both electrodes 1 and 3 (reference, in detection) are Ag/AgCl, conferring increased chemical stability after repeated extraction-detection cycles (see Methods). Extraction occurs within pixel *a via* electrodes 1 (cathode) of pixel *a* and 1' (anode) of pixel *b*. Next cycle, cathode and anode roles are reversed, extraction occurring in pixel *b*; thus, AgCl is periodically recycled. During detection, the counter electrode is 1.

Figure 3. **Deconstructed pixel device.** (a) **Calibration curve** for a typical Pt nanoparticle-decorated, CVD graphene-based electrochemical glucose sensor, 3 x 3 mm^2, with Ag/AgCl and Pt wires as external electrodes (Figure 2(b), panel 2). Glucose is dispensed into the 24 μL enzyme-containing reservoir, H$_2$O$_2$ produced by the glucose reaction with the glucose oxidase being detected in the chronoamperometric current recorded at 0.4 V applied to the graphene electrode against the micro Ag/AgCl reference. The hypo- to hyper-glycaemic range, after dilution in the pixel gel, maps as indicated in purple (see Methods). (b) **Glucose extraction-detection; determination of follicular vs non-follicular glucose extraction fluxes.** Glucose was extracted for 1 hour via the configuration in Figure 2(b), panel 1, at an iontophoretic current of 0.2 mA (corresponding to a current density of 2.2 mA/cm^2), and with 100 mM subdermal glucose, through (i) a single hair follicle (using a skin sample with 32 hairs/cm^2), and (ii) non-follicular skin (using a skin sample with only 6 hairs/cm^2), into two separate 24 μL enzyme-containing gel reservoirs. Panel 1: These samples were then measured by chronoamperometry by the same graphene-based sensor using the configuration from Figure 2(b), panel 2. Chronoamperometric current baselines were also recorded before RI in both cases. Panel 2: After subtraction of the respective baselines, average values of the detected current, I$_1$ and I$_2$, were determined over the 50 to 600 s range, respectively. Then, in reference to the detection current-concentration calibration curve of the sensor, the concentrations of glucose C$_1$ and C$_2$ for the two cases were determined by interpolation (see also Methods). Subsequently, these values, reflecting the concentration of extracted glucose after dilution in the volume of the pixel gel, were used to calculate follicular and non-follicular extraction fluxes (Methods).

Figure 4. **A functional, fully integrated, CVD graphene-based 2 x 2 pixel array on a flexible substrate.** (a) Array realization. Panel 1: Complete layout, comprising electrodes for extraction-detection, sensing regions (Pt nanoparticle-decorated graphene of 2 mm^2 each), and an elastomer membrane with perforations (panel 2) within which a glucose oxidase-encasing hydrogel was deployed forming extraction regions of about 6 mm^2 each (dashed contours, panel 3). Electrodes 1 to 3 participate in extraction-detection (4, unused). (b) Panel 1: Linear response (Methods) of pixel sensor to 0.006 to 0.7 mM glucose. Panel 2: Response to glucose (red), PBS (cyan), acetaminophen (teal) and ascorbic acid (purple) for in-gel concentrations shown in inset (see also Supplementary, Figure S12). (c) 10 mM subdermal glucose was extracted across porcine skin *ex vivo* for 5 minutes under ~0.5 mA/cm^2 RI current. Panel 1: Sensitivity calibration curves (raw chronoamperometry data in Supplementary, Figure S9) for the 4 pixel devices, demonstrating very similar current-concentration dependencies. Targeted concentration operational range (Methods), in purple. Panel 2: Detected current *versus* time after glucose extraction within each of the four pixels characterized in panel 1; number of follicles targeted by each of the pixels is indicated; PBS

extraction used as a negative control (black baseline). Inset: averaged detected current correlated with in-gel glucose concentrations. Panel 3: Detected current *versus* time after extractions using the same pixel device for 10 and 100 mM subdermal glucose concentrations, respectively. Extracted, in-gel glucose concentrations agree with calculations based on the follicular extraction flux and the number of follicles probed (Methods; Supplementary, Figure S11). (d) An example of visual correlation between number of follicles probed by each array pixel (6mm^2 extraction area, dashed contour, over skin with ~28 follicles/cm^2), panel 1, and current detected after extraction of 10 mM subdermal glucose, panel 2. Array electrodes are visible through the skin.

Figure 5. **Second generation, screen printed, 2x2 array. (a) *Ex-vivo* (porcine skin) testing over the hypo-to-hyper glycaemic range.** Panel 1: Chronoamperometric detection curves after 5 minutes of extraction at 0.5 mA/cm^2 current density across 6 mm^2 extraction area, and subdermal glucose concentrations spanning the hypo-to-hyper glycaemic range; extraction through 2 hair follicles into ~2 μL of gel (equivalent to 1 hair follicle per 1 μL gel). Panel 2: Proportionality of the read-out current (i.e., the detection current averaged over the 50 to 600 s range) to the subdermal concentration. Panel 3: The read-out current maps onto the linear calibration curve, yielding "in-gel" glucose concentrations C_1* to C_4* in agreement with the follicular extraction flux determined from Figure 4. **(b) *In-vivo* continuous glucose monitoring on healthy human subjects.** Panel 1: Screen printed array fixed onto volunteer's forearm, and connected to a potentiostat. Array layout and components same as in Figure 4(a), panel 1; additionally, an electrically insulating layer (green) covers all interconnects, underlying the perforated elastomer membrane aligned on top of it. Panel 2: Example of chronoamperometric detection curves (corresponding to various blood glucose concentrations), acquired during alternating 5 minutes periods of extraction-detection (Methods); shorter detection times than used in Figure 4 enabled good tracking of the blood glucose profile shown in Panel 3. Panel 3: Two pixels (*a* and *b*) worked in tandem (ensuring periodic AgCl recycling in each pixel (Methods)), alternatingly delivering read-out values of ISF-borne glucose. For each pixel, a larger RI current density (~1 mA/cm^2) was used to extract glucose through 2 follicles into ~3 μL gel (the larger extraction current compensates for the larger pixel gel volume; compare with our benchmarking parameters of 1 follicle per μL of gel and 0.5 mA/cm^2 extraction current density), see Figure S17(a). Finger-stick measurements of blood glucose were taken before each extraction.

Methods

1. Materials and device fabrication.

Planar thin film/CVD graphene array.

CVD Graphene wet transfer onto a polyethylene terephthalate (PET) sheet. CVD-synthesized graphene, grown on a copper substrate, was transferred onto a flexible, previously polished PET sheet using a standard wet transfer procedure[40]. For a 2 x 2 array, four such graphene patches (larger than the final, desired size) were placed on the PET sheet roughly in the desired locations using a stencil mask (designed for subsequent electrode and track definition) to guide alignment. The graphene patches provide the working electrodes for each of the pixels of the array in the electrochemical detection of glucose. To prevent potential structural discontinuities/tearing in the graphene layer (occurring either during CVD growth or as the result of mechanical stress during the transfer procedure) leading to electrical discontinuity, a second graphene layer was subsequently transferred on top of each of the original patches.

Electrode and track deposition through physical vapour deposition (thermal and e-beam evaporation). To deposit thin film electrodes with a defined geometry, sets of polyimide industrial tape (Kapton®), laser-machined stencil masks were placed successively and aligned on top of the PET-supported graphene patches. The stencil mask sets were tailored to the array layout. To complete the reference/counter Ag/AgCl electrodes, a 500 nm silver film was deposited on top of a 20 nm palladium layer previously deposited to promote adhesion of the silver layer, followed by a 500 nm thick AgCl layer. Such thick layers of Ag and AgCl are needed to ensure a long lifetime of the reference electrode[41].

Choice of materials for extraction and electrochemistry electrodes. *Extraction:* Ag/AgCl has been chosen as the material for the extraction electrode couple due to the ability of AgCl to recover its surface chemical composition after electrochemical stress, hence ensuring its stability after repeated cycles of extraction-recovery that require the electrode polarity to alternate. It was found that after four extraction-detection cycles performed with the array, the potential across the Ag/AgCl electrodes changed negligibly (by only ~30 mV), establishing their recovery. *Detection:* One of the extraction electrodes was then used as the counter electrode instead of Pt. In this way, the number of steps required for the array fabrication was greatly reduced, while not affecting electrochemical detection. Use of Ag/AgCl as a pseudo-reference is well-documented[28,42]; here, its stability was verified in potentiometric experiments relative to a standard saturated calomel electrode (SCE).

Graphene patterning. The graphene patches defining the sensing areas were then patterned in the pre-defined geometry (e.g., into 1 x 2 mm^2 areas according to the layouts in Figure 4). Although low energy oxygen plasma can be used to etch graphene supported by plastic substrates, mechanical cutting (using a scalpel) was successfully employed in the current realization to remove the excess graphene from the pixel patches.

Realization and transfer of an elastomer membrane designed to support the enzyme-encasing gel. Polydimethylsiloxane (PDMS) mixed with a curing agent was spin-coated on a PET support sheet and cured, leading to a ~100 µm thick membrane. Circular holes (1.5 - 3 mm diameter) or rectangles (~2 x 3 mm^2) of similar area were then cut to create sockets for the reservoir gel. After careful underwater peeling in a de-ionized water bath, the PDMS membranes were transferred onto the array with defined electrodes and tracks, ensuring alignment of the sockets to the electrochemical cell region of each pixel. The assembly was then left to dry in air.

Platinum nanoparticle deposition onto the graphene pixel electrodes. Pt nanoparticles were formed and deposited on the graphene sensing regions of the pixels through appropriate stencil masks by DC sputtering under argon. Contrary to electrodeposition, sputtering is a method that allows easy scale-up of Pt nanoparticle deposition. By tuning the argon gas pressure and sputtering time, particles with 4.5 nm mean diameter were produced. See

Supplementary, section 3, and Figure S4 for further characterization of this Pt nanoparticle-CVD graphene hybrid material.

Gel casting and enzyme entrapping (Figure 4). 1 mL of a clear 2% w/v solution of agarose in phosphate-buffered saline (PBS) at pH 7.4 was formed by warming above 80˚C and was then cast on a glass slide (allowing it to spread and flatten). The gel was left to shrink under accelerated drying in a fume hood for 10 minutes, after which blocks of gel (of ca. 1-2 μL, determined by weighing), with footprint areas corresponding to predetermined pixel regions, were excised. Then, 0.5 to 1 μL of enzyme (12 mg/mL) was placed on and absorbed into the electrode side of the gel blocks. Finally, the gel blocks were positioned on top of the individual pixels, inside the sockets of the PDMS membrane, and glucose subsequently extracted into them. Once in contact with the skin (and sandwiched between the skin and the surface of the device), the gel did not shrink any more over the duration of extraction and detection experiments presented in Figure 4; this was confirmed by peeling and weighing the gel at the end of the experiment.

Screen printed array

Realization and characteristics. Screen printed arrays (Figure 5(b), panel 1) were commissioned commercially with the same architecture as in Figure 4(a), using an Ag/AgCl ink (DuPont 5874), and a graphene-based ink (HDPlas® Graphene Ink IGSC02002 from Haydale Ltd., UK). The process allowed the thickness of the Ag/AgCl electrodes to be increased to ~ 6 μm, with the aim of increasing the stability and lifetime of the pixel devices. A biocompatible, electrically insulating layer (~1 μm thick) was also printed around the active areas of the pixel devices, covering the conductive tracks of the array. Pt nanoparticles were deposited, using stencil masks, in similar conditions as described for the thin film/CVD graphene arrays. A PDMS layer, as described above, was then aligned with the active areas of the devices, and the array was completed by placing gel patches on top of the active areas. The gel composition was changed (see below), to improve stability (and maintain volume) during long term operation.

Gel formulation (Figure 5). An agarose-glycerol-water hydrogel was prepared by dispersing agarose (2.5 wt %) within an aqueous solution of glycerol (50 wt % in 0.1 M PBS (pH 7.4)). The dispersion was first stirred at 50°C for one hour to allow sufficient swelling, then heated at 95 °C for another hour to ensure complete agarose dissolution, and finally cooled down to 50 °C prior to pouring it between two glass slides to allow the formation of a thin film. Once jellified, the gel was excised using a razor blade according to the pixel dimensions. The addition of glycerol as co-solvent increased the stability of the hydrogel by delaying water loss during pixel device operation, and without compromising its performance during both extraction and detection.

This new formulation was used in all the *ex-vivo* and *in-vivo* experiments presented in Figure 5. The gel is stable (decreasing by ~10 to 15%) when in contact with the skin over ~6 hours of continuous glucose monitoring *in-vivo*, as shown in Figure 5, panel 3; the robust structure of the gel is still evident when the experiment is terminated (see Supplementary, Figure S17(b)). Beyond this proof-of-concept, we are pursuing development and optimization of more advanced gel formulations.

2. Calibration of pixel sensors. Interference tests.

Calibration via glucose additions to the gel. To completely characterise a generic sensor (whether in a deconstructed configuration as in Figure 2(b), or in a pixel within an array), a chronoamperometric current *versus* glucose concentration calibration curve was established. In chronoamperometry, the change in the electrochemical current with time is tracked at the working electrode, as a function of increasing glucose concentration, at a fixed applied potential (here, 0.4V) against an Ag/AgCl electrode. A constant volume of increasingly concentrated glucose solutions (in PBS) was successively added, at regular intervals, to the enzyme-containing gel reservoir (raw chronoamperometry data in Supplementary, Figures S6 and S9), and the increase in the catalytic current relative to the background (i.e., in the absence of glucose) was determined; an average of 10 readings in the plateau region of

the current step were recorded for this purpose. For the pixel array devices, delivery on top of the counter electrode mimics the glucose path during actual extraction conditions (see description of extraction circuit in Figure 2(c)), while at the same time allowing the system to stabilize after each glucose addition. Reservoirs larger than 3 μL are preferable to minimise occasional current transients associated with mechanical effects due to manual delivery of analytes. All calibration experiments were performed in a glove box in conditions of high humidity to prevent shrinking of the gel reservoirs. From five successive, replicate calibration curves obtained with the *same device*, the standard deviation in the data broadly equated to 10 to 12% of the corresponding mean. We attribute this variability to pipetting accuracy and to small variations in the original pixel gel volume. We use this error across all the calibration data presented in this work. Having established similarity in the response of several batches of devices, for the routine characterization of similarly produced sensors, fewer glucose concentrations were used to create the calibration curve.

Correlation between calibration curve and chronoamperometric detection current. We have verified that the averaging procedure over the time interval mentioned in the main text of the chronoamperometric detection current produces values that match well the calibration curves obtained from step glucose additions to the pixel gel. Figure 5(a), panels 1 to 3 present an example of such good correlation.

Interference tests with pixel arrays. Acetaminophen, ascorbic acid, and uric acid were tested as potential interferants to glucose detection (though only acetaminophen is expected to be extracted within the pixel reservoirs by reverse iontophoresis, see main text). Throughout the experiments on pixel arrays, additions to the gel reservoirs created physiologically pertinent interferant-to-glucose ratios; the smallest concentration of interferant delivered to the pixel reservoirs was close to the limit of detection of our pixel devices (Supplementary, Figures S12-13). C_S, the subdermal glucose concentration, corresponding to C, the in-gel concentration, can be determined via the relationship $C_s = C \cdot F^{-1} \cdot \left(V\left[\mu L\right] / 1\left[\mu L\right]\right)$, where V is the volume of gel reservoir, and F is the "subdermal-to-in-gel" conversion factor evaluated for 1 μL of gel. For a single follicular path, and extraction conditions used throughout this work for the pixel arrays, F was estimated to be about 2.4 x 10^{-3} (see main text). Further data and related discussion can be found in Supplementary (see Figures S12-13).

3. Limit of detection (LoD), sensitivity, and operational range

The LoD of a generic sensor (in a deconstructed configuration or in a pixel within an array) was determined from the relationship $LoD = 3.3 \cdot \sigma / S$ [43,44], where σ is the standard deviation of the noise (as determined from the raw chronoamperometry data from Figures S6 and S9, Supplementary), and S is the slope of the sensor's linear calibration curve (e.g., as determined from Figures 4(b), panel 1, 5(a), panel 3, or Supplementary, Figure S7). Sensitivity was defined as the slope of the sensor's calibration curve (e.g., as shown in Figures 4(b), panel 1, or Figure S7 in Supplementary) normalized to the geometrical area of the pixel electrode (i.e., 3 x 3 mm^2 for the deconstructed pixel device, and 1 x 2 mm^2 for electrode 2 in Figure 4(a), panel 1); further relevant discussion can be found in Supplementary, section 7. The operational range for the glucose concentration in the pixel gel C can be established using the relationship $j \cdot \Delta t \cdot I \cdot N = C \cdot V$, where j, the glucose extraction flux (see below), scales with the subdermal glucose concentration spanning the hypo- to hyper-glycaemic range; N is the number of hair follicles through which extraction takes place. The operational range can be adjusted by varying parameters such as Δt and I, the extraction time and current, respectively, as well as V, the volume of the pixel gel (equal to the active (extraction) area of the gel multiplied by the thickness of the gel).

4. Determination of follicular vs non-follicular glucose extraction fluxes.

The procedure described in Figure 3(b) allowed C_1 and C_2, the glucose concentrations within the pixel gel corresponding to follicular and non-follicular extraction, respectively, to be determined. Using these values, and the relationship $j \cdot \Delta t \cdot I \cdot N = C \cdot V$, as above, the follicular and non-follicular glucose extraction fluxes were determined. The values obtained are proportional to the subdermal glucose concentrations (100 mM in the data from Figure 3), and scaling is therefore required when the subdermal concentration changes. The follicular and non-follicular fluxes reported in the main text were scaled to 10 mM subdermal glucose concentration. Data from Figure 4 (corresponding to the planar thin film/CVD graphene arrays) were used to independently determine a value for the follicular extraction flux (see main text). This also allowed one to determine whether the extraction geometry of the planar pixel array has an influence over the extraction process.

5. Extraction-detection cycle with a pixel array.

Ex-vivo experiments. Fresh abdominal pig skin was dermatomed (Zimmer®, Ohio, USA) to a nominal thickness of 750 μm and then cut into suitably-sized pieces, before being frozen until used. In contrast to the deconstructed device in Figure 2(b) (see also Supplementary, section 4), the anode and cathode now contacted the skin on the same side (Figure 2(c)) making the measurement truly non-invasive. The dermatomed pig skin was placed over the sensor, with the external side in direct contact with the pixel array, while the subdermal side faced the operator allowing the alignment of the gel reservoir regions (i.e., the active areas of the pixel devices) to the clearly visible follicles (made possible by the partial transparency of the skin). Buffer-saturated absorbent tissue was used as the subdermal compartment in which glucose solution was dispensed. A piece of paraffin film was placed over the impregnated tissue and pressure was applied to ensure contact between the skin and the gel reservoirs. We did not specifically perform an analysis of behavior under stress but, in the current conditions, the extraction results are reproducible and compatible with what is expected from glucose flux estimations. Hence, stress, at least thus far, does not negatively affect the operation of the device.

Glucose was extracted under a current density of ~0.5 mA/cm^2 for 5 minutes into the gel reservoir (1-2 μL in volume, ~6 mm^2 in cross section) using an Ag/AgCl electrode couple provided by two adjacent pixels, and detected for 10 minutes. Once the extraction was completed, glucose detection was performed (procedure described in Figure 3) without changing the sensor position. No significant gel volume variation was recorded in these experiments, when the gel was sandwiched between the pig skin and the device surface, and laterally confined by the PDMS membrane. Cathode and anode of the iontophoresis circuit are provided by two different pixels and alternate from cycle to cycle (see Figure 2 (c)). Thus, the "two pixel" extraction-detection cycle follows the following steps: (1) extraction in pixel _a,_ accompanied by depletion of AgCl from pixel _a_ electrode (the cathode in the electrochemical reaction); (2) detection of extracted glucose by chronoamperometry in pixel _a_; (3) pixel _a_ gel cleaning: with a high glucose subdermal concentration (e.g., 100 mM), two or three chronoamperometry detection cycles are performed to completely deplete the extracted glucose from the gel; and (4) glucose extraction in pixel _b,_ accompanied by the recovery of the AgCl surface layer of pixel _a_ electrode (now the anode in the electrochemical reaction).

In-vivo experiments. The protocol (REACH EP 17/18 94) was approved by the University of Bath Research Ethics Approval Committee for Health. Healthy, non-diabetic volunteers underwent an overnight fast, and the area of the forearm where the sensor would be applied had been carefully shaved and cleaned. The array was strapped onto the skin with mild pressure, as shown in Figure 5(b), panel 1. Good contact between the skin and the device is indicated by a low resistance during RI extraction. In such conditions, the device works within the expected parameters, and in agreement with all the other results in the paper. The sensor was first 'stabilized' by performing several chronoamperometric detection cycles without RI extraction until the results superimposed. Concurrently, blood glucose concentrations were measured via conventional "finger-sticks" at regular intervals (using a commercial

glucose meter, Accu-Chek® Mobile). Subsequently, the subject consumed a carbohydrate-rich meal (~200 g of pasta), triggering the expected response in blood glucose concentration (i.e., a clearly perceptible increase in glycaemia followed by its normalisation in response to insulin secretion) over the next 2 - 2.5 hours. Then, the subject consumed a snack containing ~60 g of sugar and the change in blood glucose was followed as before for a further period of about one hour. During this provocation of changes in blood glucose levels, RI extraction and electrochemical detection cycles were performed every 10 minutes (the detection stage having been reduced from 10 minutes to 5 to permit collection of more frequent data points). Measurements with two pixels, working in tandem, were alternated as detailed above. The RI glucose signal versus time profile in Figure 5(b), panel 3, in this case, did not use the read-out current averaged over 50 to 600 s (as employed in the rest of the work), but instead employed the instant current detected at t = 300 s. This alternative method of displaying the output data from the device clearly tracked with fidelity the variation in blood glucose concentration. Notably, both the instant measurement (at t = 300 s, in this case) and the averaged current correlated similarly with the subdermal concentration, as shown in Supplementary, Figure S18. With the current pixel characteristics and dimensions, measurement time sequence, and overall monitoring period, we did not observe glucose accumulation in the pixels and the lack of "memory effect" is also supported by the *ex vivo* results in Figure 5(a). After extraction, complete glucose conversion to H_2O_2 is anticipated due to the excess quantity of enzyme in the pixel gel; in addition, with the 15-minute delay between each detection step within that pixel (i) there is no concern about analyte diffusion-limitation as the pixel size is so small, and (ii) disproportionation of any residual H_2O_2 (leading to pixel "clearing") is expected, catalysed by the Pt[45] and Ag nanoparticles[46] (present in the screen printed ink) of the various electrochemical electrodes. No perceptible discomfort was perceived by the volunteers during the extraction. Only mild tingling under the extraction electrodes was transiently (a few seconds) experienced at the beginning of current passage. Further, no skin irritation was observed after the 6-hour *in-vivo* glucose monitoring experiments reported in Figure 5 (Supplementary, Figure S17 (a)).

The data that support the plots within this paper and other findings of this study are available from the corresponding author upon reasonable request.

References

40.   Li, X. et al. Transfer of large-area graphene films for high-performance transparent conductive electrodes. *Nano Lett.* **9,** 4359-4363 (2009).

41.   Polk, B. J., Stelzenmuller, A., Mijares, G., MacCrehan, W. & Gaitan, M. Ag/AgCl microelectrodes with improved stability for microfluidics. *Sens. Actuators B Chem.* **114,** 239-247 (2006).

42.   Gao, W. et al. Fully integrated wearable sensor arrays for multiplexed in situ perspiration analysis. *Nature* **529,** 509-514 (2016).

43.   Shrivastava, A. G. & Vipin B. Methods for the determination of limit of detection and limit of quantitation of the analytical methods. *Chronicles of Young Scientists* **2,** 21-25 (2011).

44.   *Bioelectrochemistry: Fundamentals, Applications and Recent Developments* (Wiley, Hoboken, 2011).

45.   Petrucci, R. H. *General Chemistry: Principles & Modern Applications*, 9 edn. (Prentice Hall, Upper Saddle River, 2007).

46.   He, D., Garg, S. & Waite, T. D. H_2O_2-mediated oxidation of zero-valent silver and resultant interactions among silver nanoparticles, silver ions, and reactive oxygen species. *Langmuir* **28,** 10266-10275 (2012).
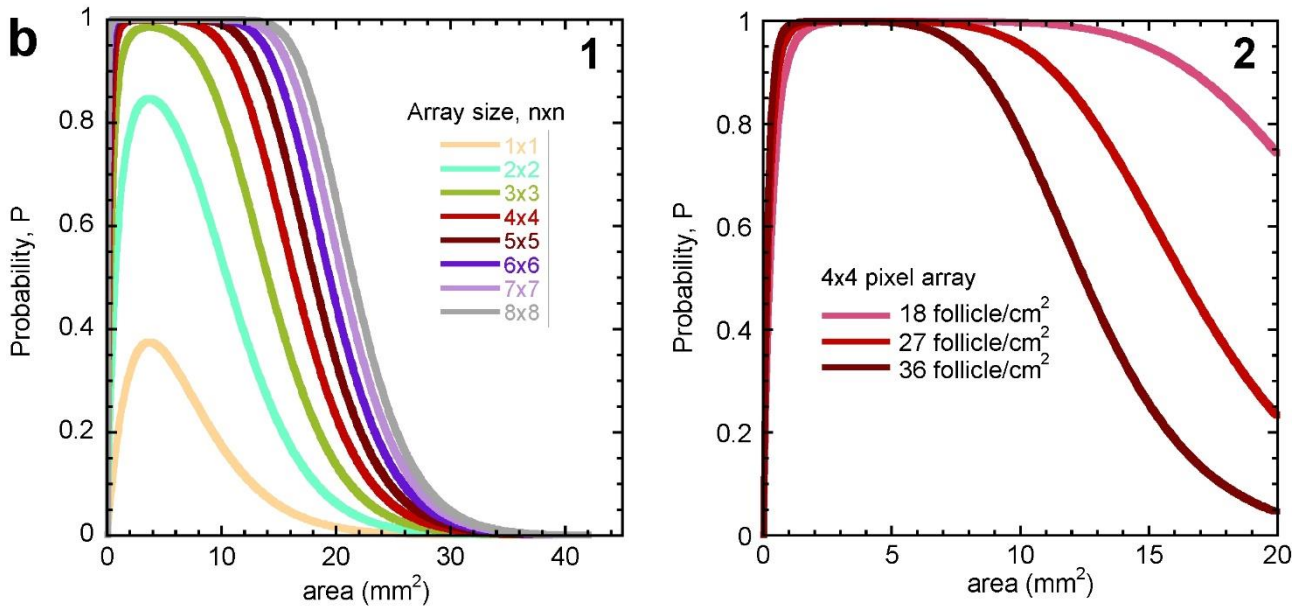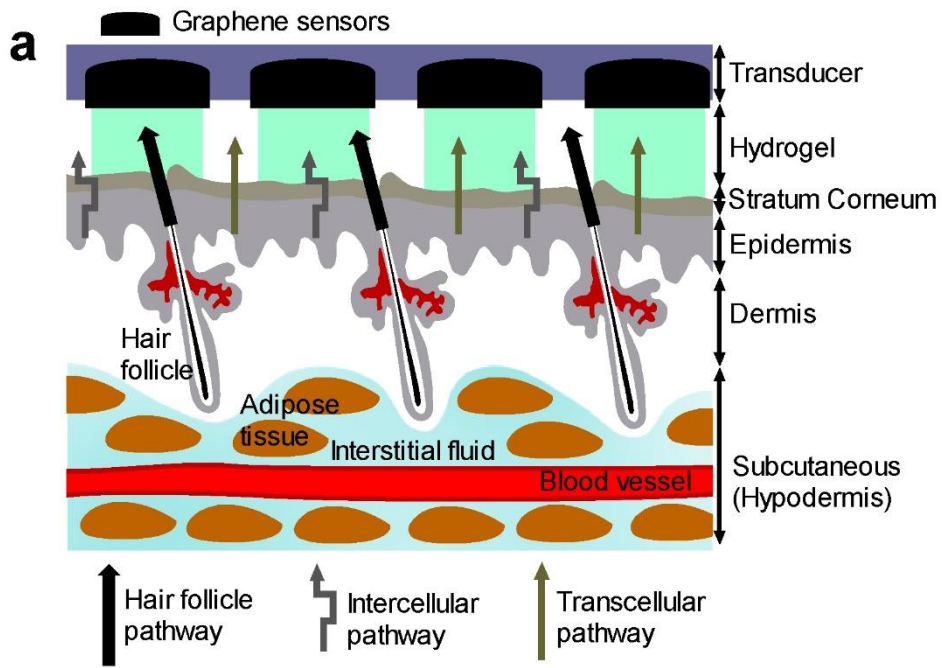
a

Graphene sensors

Transducer

Hydrogel

Stratum Corneum

Epidermis

Dermis

Hair follicle

Adipose tissue

Interstitial fluid

Blood vessel

Subcutaneous (Hypodermis)

Hair follicle pathway

Intercellular pathway

Transcellular pathway

b

1

Probability, P

Array size, nxn
- 1x1
- 2x2
- 3x3
- 4x4
- 5x5
- 6x6
- 7x7
- 8x8

area (mm^2)

2

Probability, P

4x4 pixel array
- 18 follicle/cm^2
- 27 follicle/cm^2
- 36 follicle/cm^2

area (mm^2)

Figure 1

19

a

Flexible substrate

1 2 3

Graphene + nanoparticles

4

Gel/enzyme reservoir

Elastomer

Hair follicle

Skin

b

Cathode (Ag/AgCl)

Anode (Ag)

Enzyme reservoir

Porcine skin & hair follicle

+G +G +G +G

①

Franz cell

PBS & glucose (G)

Cathode: AgCl(s) + e⁻ → Ag⁰(s) + Cl⁻(aq)

Anode: Ag⁰(s) + Cl⁻(aq) → AgCl(s) + e⁻

c

Flexible substrate

c

d

2 3 3'

a b 2'

1 1'

Elastomer

Porcine skin

PBS & glucose

Cathode: 1, on pixel a; Anode: 1', on pixel b

Alternate cycle: cathode and anode invert

Ag/AgCl

Pt

Gel/enzyme reservoir

Elastomer

②

Ag

Graphene + nanoparticles

SiO₂/Si

Figure 2

20

Cathode: $AgCl(s) + e^- \rightarrow Ag^0(s) + Cl^-(aq)$

Anode: $Ag^0(s) + Cl^-(aq) \rightarrow AgCl(s) + e^-$

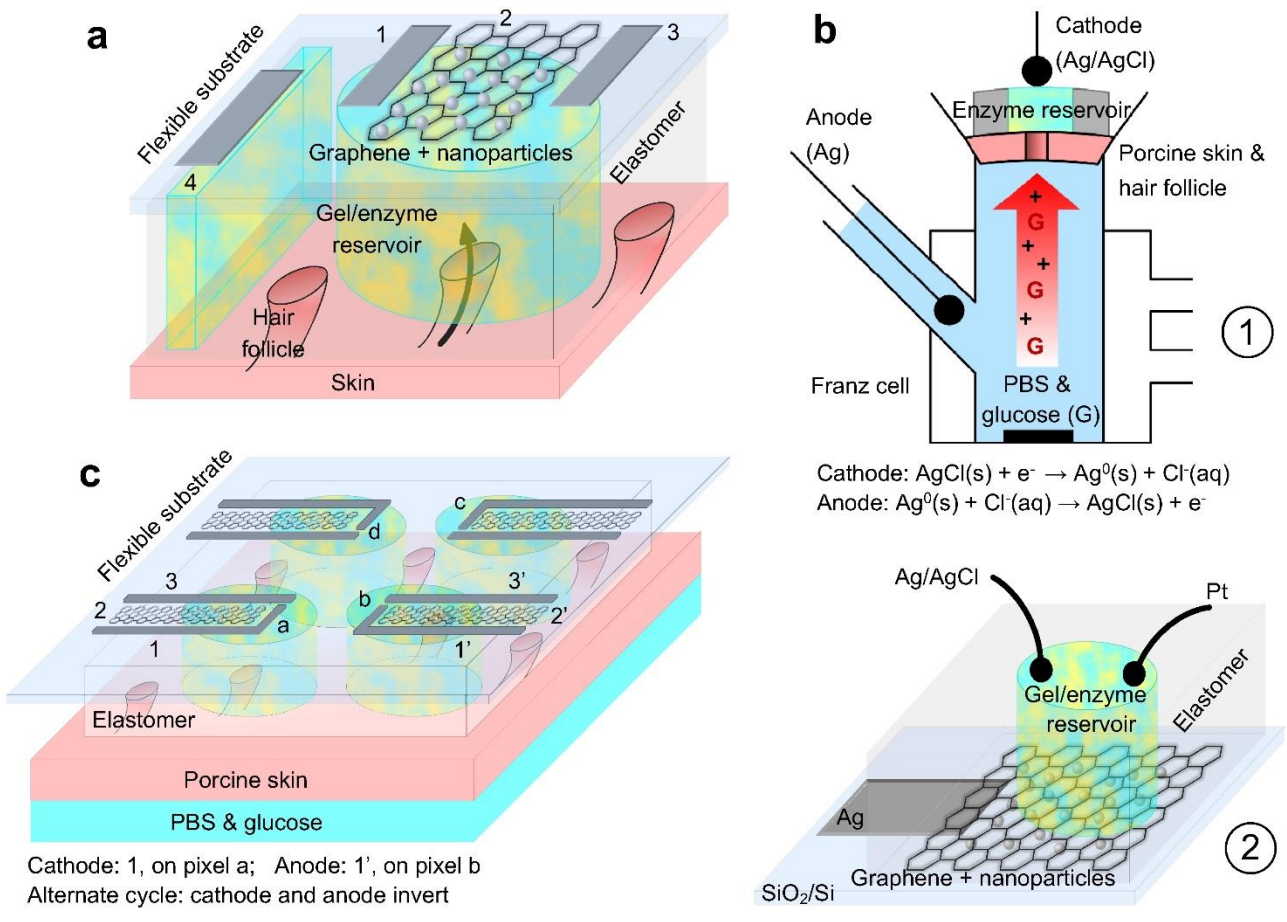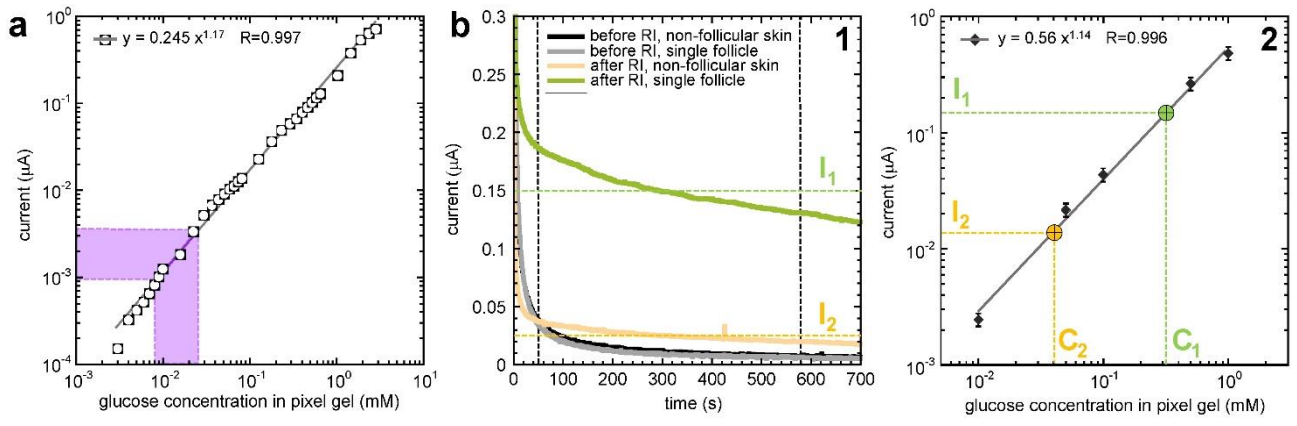Cathode: 1, on pixel a; Anode: 1', on pixel b
Alternate cycle: cathode and anode invert

Figure 2

Figure 3

Figure 4

Figure 5